URTeC: 2902747

Imaging Pyrite Oxidation and Barite Precipitation in Gas and Oil Shales

Qingyun Li[1,2], Adam D. Jew*[1], Andrew M. Kiss[1], Arjun Kohli[1,2], Abdulgader Alalli[2], Anthony R. Kovscek[2], Mark D. Zoback[2], David Cercone[3], Katharine Maher[2], Gordon E. Brown, Jr.[1,2], John R. Bargar[1];
1. Stanford Synchrotron Radiation Lightsource, SLAC National Accelerator Laboratory, 2. School of Earth, Energy & Environmental Sciences, Stanford University, 3. National Energy Technology Laboratory, Strategic Center for Natural Gas and Oil.

Abstract

The complex suite of chemicals that comprises fracture fluid may result in chemical alterations of shale matrices, which can in turn affect gas and oil transport through the matrices and across fracture-matrix interfaces. In this study, we examined chemical reactions in carbonate-poor Marcellus and carbonate-rich Eagle Ford matrices upon reaction with synthetic fracture fluid (initial pH = 2) at 77 bar and 80 ^{o}C for three weeks. A subset of the experiments was conducted with additional Ba^{2+} and SO_4^{2-} ions in the fracture fluid to promote barite precipitation. Micro-CT and synchrotron x-ray fluorescence microscopy were used to identify the reaction zones in shale. In contrast with previous studies that focus on chemical reactions at the shale-fluid interface, we observe that the chemical reactions can penetrate a considerable distance into the shale matrix unless the matrix is devoid of any microcracks. The results show that, for shale cores with microcracks, both pyrite oxidation/dissolution and barite precipitation can extend millimeters into the matrix, depending on mineral compositions of the shale. Following 3 weeks of reaction, the carbonate-poor Marcellus system had final pH of 4. The altered zone of the shale core showed a pyrite oxidation zone > 5 mm into the matrix, while barite precipitation was limited to the surface (≤ 45 μm into the matrix). Conversely, the solution of the carbonate-rich Eagle Ford cores was completely neutralized during reaction. When compared to Marcellus, the Eagle Ford shale had a reversed trend with limited pyrite oxidation, and extensive barite precipitation (several millimeters into the matrix) in microcracks and in matrix pores. This comparison is consistent with earlier findings that compared to low pH, near-neutral pH promotes barite precipitation and Fe(II) oxidation. Our results also suggest that scale precipitation, even if formed only at the fracture-matrix interface, can limit transport of dissolved oxygen across the interface, and may also affect transport of gas and oil from shale matrices to fractures for recovery.

Introduction

Liquid fracture fluids at high pressure are used to fracture unconventional shale formations to increase the simulated rock volume to increase gas and oil recovery. After shale is fractured, gas and oil can transport through shale matrices to fractures, eventually travelling to pipelines and production wells. However, current simulation practices extract only < 25% of gas and < 10% of the oil estimated in the formation (Kuuskraa et al. 2013), and it is hypothesized that low matrix diffusivity might contribute to the low overall recovery efficiency (Karra et al. 2015). Geophysical studies have demonstrated that hydrocarbon flow through shale matrices is affected by different rock compositions and pore structures, and involves complex transport mechanisms such as Knudsen diffusion, slip flow, and gas adsorption/desorption (Fathi et al. 2009, Villazon et al. 2011, Swami et al. 2012, Heller et al. 2014, Guo et

al. 2015, Zhang et al. 2015, Al Ismail et al. 2016, Huang et al. 2016, Wu et al. 2017). From the perspective of geochemistry, both mineralogical composition and pore structure of shale matrices can be altered by chemical reactions, affecting hydrocarbon flow in shale matrices. However, experimental studies of shale chemical alterations when exposed to fracture fluids have been limited. Existing studies have focused mostly on shale fracture surfaces, sand and chip surfaces, and evolution of aqueous fluids. These studies have shown that important shale chemical reactions include the dissolution of primary minerals such as carbonate and pyrite, and precipitation of secondary minerals such as carbonate, sulfate, and (hydr)oxides (Grieser et al. 2007, Pournik et al. 2014, Dieterich et al. 2016, Harrison et al. 2017, Jew et al. 2017, Marcon et al. 2017, Vankeuren et al. 2017). Although these studies provide insights to gas/oil and fluid transport behavior through fractures, they cannot be readily applied to estimating chemical alterations more than tens of micrometers into the shale matrix. If these chemical reactions occur inside the shale matrix, they can alter pore structures which are critical for gas/oil transport and production.

The limited knowledge regarding shale matrix alterations by fracture fluid is likely due to its extremely low permeability that limits aqueous fluids to flow through. However, considerable water imbibition can occur within a few days (Dehghanpour et al. 2012, Dehghanpour et al. 2013, Gu et al. 2015), a much shorter timescale than typical shut-in periods (3–6 weeks) before production commences. In fact, only 20–40% of the injected fracture fluid volume can be recovered as flowback water, with the rest remained in the formation. Once the fracture fluid is imbibed, the various chemicals it contains, including acids and dissolved oxygen, can lead to chemical reactions inside shale matrices where large quantities of gas and oil are trapped. Nevertheless, the length scale of the penetration of chemical reactions into shale matrices is largely unknown, and thus it is difficult to estimate the sensitivity of the chemically damaged zone to various factors, such as rock microstructure and fluid properties.

In this study, we imaged the depths to which these chemical reactions occur in various types of shale matrices, and identified the factors that control the alteration depths. Two important chemical reactions we focused on were pyrite oxidation and barite precipitation. Barite ($BaSO_4$), a commonly found precipitate associated with scaling, results in significant economic loss during hydrocarbon production (Kan et al. 2012). The concentration of Ba in flowback water is typically high and the solution is usually over-saturated with barite (He et al. 2014). Additionally, Fe released from pipeline corrosion, pyrite dissolution, and siderite dissolution can lead to precipitation of Fe(III) (hydr)oxides as another type of scale mineral (Moghadasi et al. 2003, Jew et al. 2017). Unlike barite precipitation, the formation of Fe(III)-bearing scale is a redox process. Pyrite (FeS_2), a common mineral in gas/oil shales, can be oxidatively dissolved by oxygen in the fracture fluid:

$$FeS_2(s) + 3.5\ O_2(aq) + H_2O \rightarrow Fe^{2+} + 2\ SO_4^{2-} + 2\ H^+ \quad \text{Eq.1}$$

The Fe(II) released during pyrite oxidation can form new secondary phases, or be further oxidized to Fe(III) and precipitate as (hydr)oxides (e.g., $Fe(OH)_3$) that, before well crystallized, have larger overall volume and large metal sorption capacity compared to pyrite:

$$Fe^{2+} + 0.25\ O_2(aq) + H^+ \rightarrow Fe^{3+} + 0.5\ H_2O \quad \text{Eq.2}$$
$$Fe^{3+} + 3H_2O \rightarrow Fe(OH)_3(s) + 3H^+ \quad \text{Eq.3}$$

We show that both barite precipitation and pyrite oxidation can occur inside the shale matrices, and therefore it is necessary to consider the shale matrix as a chemically reactive medium, despite its low permeability. The deep penetration of these chemical reactions may lead to change in permeability and wettability of the shale matrix, thus altering the hydrocarbon recovery efficiency.

Methods

In order to ascertain the depths and types of chemical alterations occurring in the shale matrix, a set of shale cores was reacted with simulated fracture fluid and analyzed using a variety of laboratory- and synchrotron-based techniques (Figure 1). Three types of shale with varying mineralogical compositions were used in this study. Two types of the Marcellus shale: (1) an outcrop sample of New York Marcellus (Marcellus-NY) and (2) a core sample of Pennsylvania Marcellus (Marcellus-PA) from Eastern Gas Shales Project well PA-5 in Lawrence County (collection depth of 1258 m) (Carter et al. 2011). Both Marcellus shale samples are characterized by high clay and low carbonate contents, but the Marcellus-PA contained microcracks, while Marcellus-NY was devoid of these

microcracks as observed with μ-CT imaging. This structural variation between the two Marcellus samples is important because it provides insight into the importance of microcracks as a major type of connected porosity, while eliminating variations in shale reactability that could be caused by variations in mineralogy/organics. The Eagle Ford shale sample from southwest Texas (collection depth 3353 m) is a high carbonate rock and contains microcracks. From each shale sample, two cores (1 cm diameter, 1.5 cm long) were drilled parallel to bedding. These two cores were drilled next to each other so that they had approximately the same bedding layers to minimize the effects of heterogeneity. A slice of the shale core was trimmed from the end of the core to be analyzed for pre-reaction mineralogy using synchrotron x-ray fluorescence microprobe (μ-XRF) and powdered x-ray diffraction (XRD, Rigaku MiniFlex600 Diffractometer).

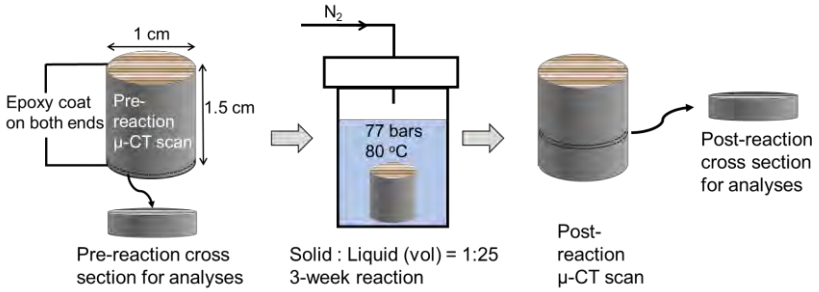

Figure 1. Illustration of experimental procedures

The two cores from each shale were reacted in synthetic fracture fluid without or with additional Ba^{2+} and SO_4^{2-} ions to promote barite precipitation. Synthetic fracture fluids were prepared in the lab with composition listed in Table 1, according to chemicals used in the National Energy Technology Laboratory's Marcellus Well E in Greene County, Pennsylvania (Hammack et al. 2014). Under the condition without additional Ba^{2+} and SO_4^{2-}, dissolution reactions were expected to dominate. For system with additional Ba^{2+} and SO_4^{2-}, 2 mM $BaCl_2$ and 0.06 mM Na_2SO_4 were added to the fracture fluid. The concentration of $BaCl_2$ was based on the Ba concentration measured from flowback water (Dieterich et al. 2016), and the concentration of Na_2SO_4 was used to generate a solution mildly saturated with respected to barite. The saturation index for barite was $\log_{10}(Q/K_{sp}) = 1.3$, where Q is the ion activity product of Ba^{2+} and SO_4^{2-}, and K_{sp} is the solubility product for barite under the reaction condition. This condition results in spontaneous barite precipitation. Before the shale cores were reacted, heat- and chemical-resistant epoxy (No. EP42HT-2, Master Bond Inc.) was applied to both ends of the cores so shale contact with fracture fluid would occur only at side walls. After the epoxy was fully cured, the cores were submerged in 30 mL of reaction fracture fluid with 15 cm^3 headspace in high temperature/pressure reactors (Parr Instruments, IL). The reactors were pressurized using ultra-pure N_2 to 77 bars and placed unagitated in an 80 °C oven for three weeks of reaction time. After reaction, solution pH was measured, and shale cores were taken out of the fracture fluid, rinsed by ultrapure deionized water, and dried at ambient condition.

Table 1. Synthetic fracture fluid chemistry. Based on NETL's Well E in Greene County, PA.

Ingredient	**Purpose**	**Percentage of Ingredient (by mass)**
Water	Base fluid	99.783%
Ethylene glycol	Scale inhibitor, iron control, Breaker	0.021%
Kerosene	Friction reducer	0.024%
Guar gum	Dry gellant	0.029%
2-Ethyl hexanol	Corrosion inhibitor for acid	0.0005%
Glycol ether	Corrosion inhibitor for acid	0.0002%
Polyethylene glycol	Biocide	0.020%
Hydrochloric acid	Acid	0.122%

Micro computed tomography (μ-CT) scans were collected from the whole cores before and after reaction using a ZEISS Xradia 520 Versa 3D x-ray microscope at 80 kV and 86 μA, with 6 s exposure time per projection. Data were reconstructed using Reconstructor Scout-and-Scan software from ZEISS. With this setup, the voxel size is 5 μm. The reconstructed tomography allows clear imaging of barite precipitation. To image pyrite oxidation, a 1 mm thick cross section was cut from the middle of each reacted core using a low-speed diamond saw. The cross sections were

imaged using synchrotron x-ray microprobe at Stanford Synchrotron Radiation Lightsource (SSRL, SLAC National Accelerator Laboratory, CA) beamline 14-3. Sulfur maps were collected (15 μm step size and 50 ms dwell time) at 2471.5 eV, i.e., at the energy where the S K-edge spectrum for pyrite has its greatest intensity. No other sulfide or disulfide species are expected to be present. Consequently, the maps at this energy provide the microscale distribution of pyrite. S maps were also collected at 2482.5 eV, which is the energy where sulfate has its greatest intensity. At this energy, all S species (including pyrite) contribute to the signal intensities on the maps. In order to remove the pyrite signal, the intensity at sulfide energy of 2471.5 eV was multiplied by 0.66 (to get the intensity contribution from pyrite at 2482.5 eV) and subtracted out of the 2482.5 eV map. Comparing the amount of oxidized form of sulfur on the post-reaction cross section versus that on the pre-reaction cross section will allow locating pyrite oxidation in the shale matrix.

Results and Discussion

The final pH of the reaction fluid is correlated with mineralogy of the shale cores. Shown in Table 2, the solution of the two carbonate-poor Marcellus shale samples remained an acidic pH throughout the 3-week reaction, whereas the carbonate-rich Eagle Ford buffered the solution to a neutral pH due to carbonate dissolution. Comparing the two Marcellus samples with similar carbonate contents, the New York Marcellus with no microcracks experienced less pH increase compared to microcrack-abundant Pennsylvania Marcellus, suggesting that microcracks provided more accessible reactive surface areas in the Pennsylvania Marcellus shale for carbonate dissolution.

Table 2. Shale mineralogical compositions in weight percentage from XRD and pH measured before and after reactions. Condition 1 refers to reactions in fracture fluid, and Condition 2 refers to reactions in fracture fluid with additional Ba^{2+} and SO_4^{2-} to form barite. XRD data were collected from pre-reaction shales, and pHs were measured at room temperature.

	Quartz	Clay	Calcite	Dolomite	Pyrite	Initial pH	Final pH Condition 1	Final pH Condition 2	Notes
Marcellus-NY	34	61	1	0	4	2.0	2.5	2.4	No microcracks
Marcellus-PA	41	41	1	6	11		4.0	3.6	Has microcracks
Eagle Ford	22	23	52	0	3		8.2	8.2	Has microcracks

Barite Precipitation

Figure 2 shows cross sectional slices of pre-reaction and post-reaction cores from μ-CT scans. The slices are roughly at the middle of each core, but are not at exactly the same location for pre- and post-reaction cores. At this resolution, secondary porosity created by carbonate dissolution are not well resolved. However, secondary precipitation of barite can be clearly observed in systems with additional Ba^{2+} and SO_4^{2-}. The two Marcellus shales have barite precipitation at the shale-fluid interfaces, whereas the Eagle Ford shale has significant barite precipitation in the microcracks (to a depth of > 1 mm) as well as in the matrix (to a depth of > 150 μm). The dramatic difference in barite precipitation between Marcellus and Eagle Ford cores correlates with the difference in solution pH between the two systems.

Previous studies and chemical modeling show that with the same initial concentrations of barium/sulfate ions in solution, barite precipitates faster and in larger amounts at near-neutral pH than at lower pH (Dove et al. 1995, Palandri et al. 2004, Steefel 2009). In the whole-core experiments in this study, both New York and Pennsylvania Marcellus shales were low in carbonate, and carbonate dissolution did not increase pH sufficiently to promote barite precipitation in the matrix. We observed that barite precipitation formed only at the shale-fluid interfaces and barely into the matrix even when there were spaces for precipitation in microcracks. This is probably because the precipitation on the core surface occluded pathways for Ba^{2+} and SO_4^{2-} to migrate into microcracks. In contrast, the large amount of carbonate in Eagle Ford resulted in complete neutralization of the acidic fracture fluid. When carbonate in Eagle Ford started to dissolve, the matrix pores and microcracks that had higher local solid-to-liquid ratio experienced faster pH increase compared to the bulk solution, resulting in faster barite precipitation in matrix pores and microcracks. The consumption of Ba^{2+} and SO_4^{2-} ions then triggered diffusion of more Ba^{2+} and SO_4^{2+} ions into the matrix, decreasing barite saturation in bulk solution so that barite precipitation on the outer surface of the Eagle Ford core is limited.

The location of barite precipitation has profound implications for unconventional operation. In carbonate-rich formations such as Eagle Ford, it is common to inject acid to open more pore space to facilitate hydrocarbon transport. There is no doubt that carbonate can rapidly dissolve upon contact with acids, but in pore spaces and microcracks, carbonate dissolution can actually promote barite scale formation due to pH neutralization and due to secondary porosity that allows barite to infill the matrix. In such cases, although the fracture aperture may be increased through acid injection, the microcracks and matrix pores, as well as the secondary porosity produced by carbonate dissolution, might actually be clogged by barite, reducing hydrocarbon transport through the matrix to fractures. Such a scenario highlights the importance of preventing barite formation even though the shale has a large amount of carbonate soluble in acids.

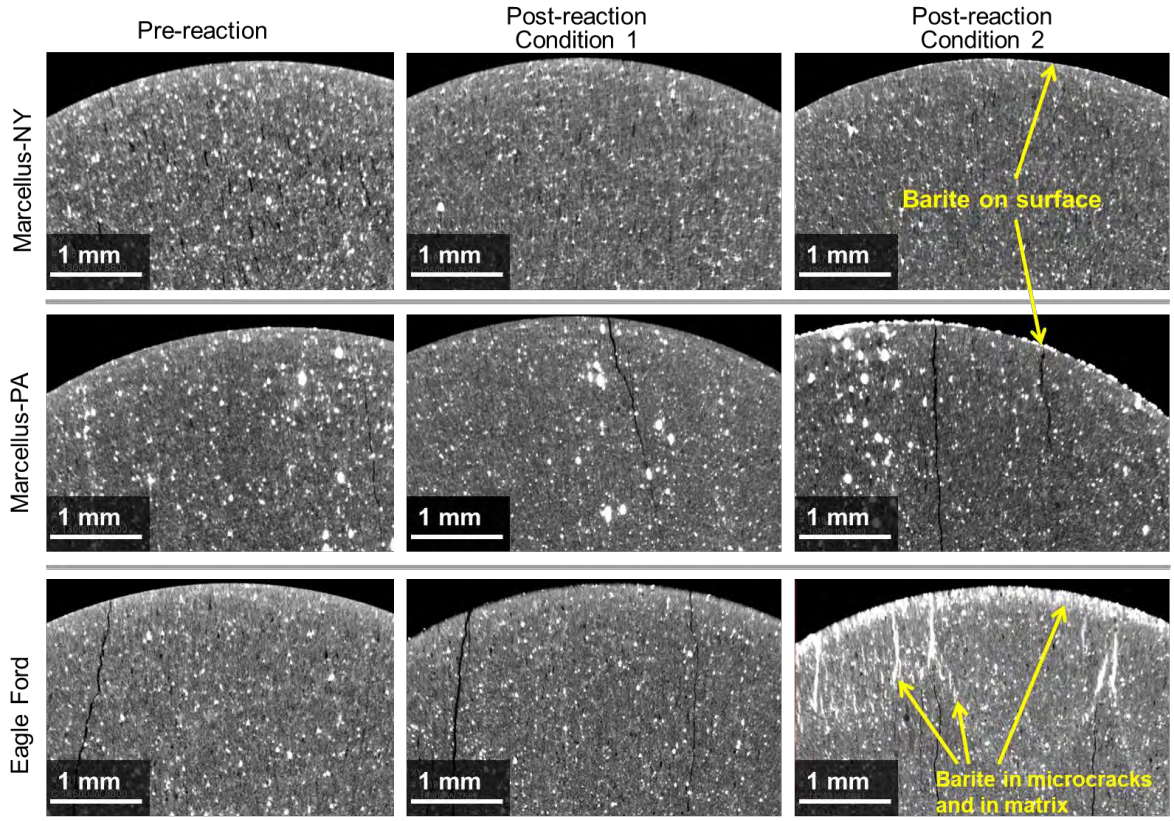

Figure 2. Cross section slices of pre-reaction and post-reaction shale obtained from μ-CT scans. Slices are roughly at the middle of each core but are not at exactly the same location. The voxel size is 5 μm. Condition 1 refers to reactions in fracture fluid, and Condition 2 refers to reactions in fracture fluid with additional Ba^{2+} and SO_4^{2-} to form barite. Brightness and contrast were adjusted for each individual slice to show features clearly.

Pyrite Oxidation

As shown in our earlier study, oxidative dissolution of pyrite leads to precipitation of Fe(III) (hydr)oxide that can occlude pore space and coat fracture surfaces (Jew et al. 2017). It is important to understand how far into the shale matrix pyrite oxidation occurs in order to understand the length scale of the reaction zone in shale where Fe(III) scale formation could occur. Figure 3 compares the sulfate maps collected from the pre-reaction and post-reaction cross sections of New York Marcellus, Pennsylvania Marcellus, and Eagle Ford. If pyrite is oxidized, the accumulation of sulfate will be indicated by a higher intensity (i.e., warmer color) in Figure 3.

There is little to no detectable difference in the S-μ-XRF maps for the New York Marcellus pre- and post-reaction cross sections (Figure 3), except that the sulfate in barite precipitation is shown at the shale surface (≤ 30 μm into the matrix), consistent with observation in the μ-CT slice for the post-reaction Condition 2 sample (Figure 2). This outcrop shale lacked microcracks and other connected pores, effectively retarding chemical reactions inside the matrix. This hypothesis is further supported by the lack of acid neutralization throughout the reaction (Table 2).

In contrast to New York Marcellus, the Pennsylvania Marcellus with microcracks experienced extensive pyrite oxidation throughout the entirety of the 1 cm core as evidenced by the appearance of sulfate in S-µ-XRF mapping (Figure 3). This finding suggests that in the presence of microcracks, dissolved oxygen can penetrate at least 5 mm (half of the 1 cm diameter of the core) into the Pennsylvania Marcellus shale cores. It is worth noting that in the post-reaction cores, pyrite oxidation occurred not only in regions close to the microcracks, but throughout the entire matrix, suggesting that in addition to microcracks, there were other connected pores in the matrix. Transport of fracture fluids and diffusion of aqueous species likely occurred through hydrophilic phases such as clay minerals. The dissolved oxygen migrated into the matrix faster than pyrite oxidation, so the majority of pyrite remained unoxidized, as confirmed by synchrotron S-µ-XRF maps (Figure 4) taken at the sulfide characteristic energy of 2471.5 eV, where hotspots are mostly due to pyrite. The dramatic difference in reactivity between Pennsylvania and New York Marcellus cores indicates that the microcracks and other connected pores are the most important factors that lead chemical reactions into the matrix.

The comparison between the two post-reaction Pennsylvania Marcellus samples reacted without and with additional Ba^{2+} and SO_4^{2-} is also striking. Although both cross sections show oxidized sulfur, the one with barite precipitation at the interface (≤ 45 µm into the matrix) has less overall oxidation. One possible explanation, as illustrated in Figure 5, is that the barite precipitation at the shale-fluid interface armored the surface, hindering transport of dissolved oxygen to the shale interior. This explanation is supported by another study done by the authors of this work, where the permeability of Pennsylvania Marcellus was measured before and after reaction in fracture fluid with additional Ba^{2+} and SO_4^{2-} (i.e., the same condition as used in this study), and the post-reaction permeability was found lower than pre-reaction permeability due to barite precipitation (Alalli et al. 2018).

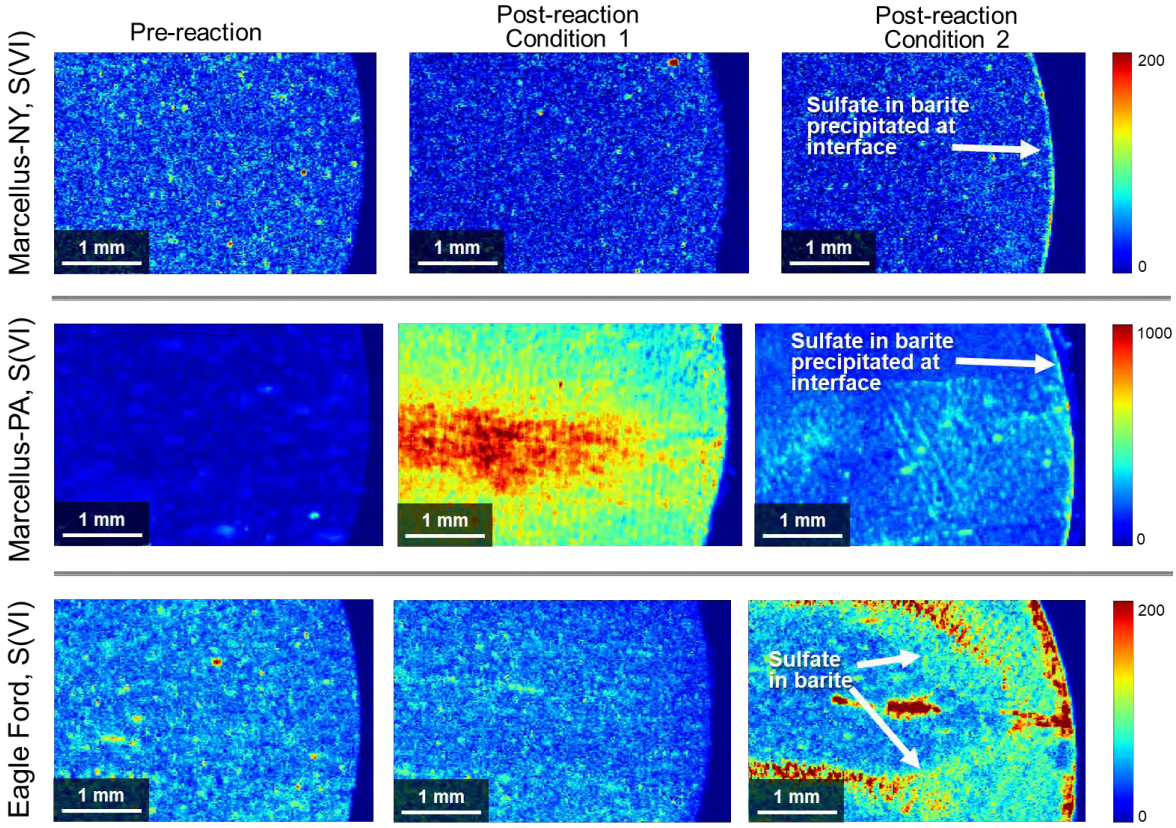

Figure 3. Synchrotron µ-XRF sulfate maps. The maps show cross sections where the edges on the right are the outer surface of the shale cores. If pyrite is oxidized, higher intensity (i.e., warmer color) will be observed in the post-reaction maps. Sulfate in barite is also observed, and is consistent with the barite locations shown in Figure 2. Pyrite oxidation is not noticeable in the matrices of Marcellus-NY and Eagle Ford, but it occurred throughout the entire matrices of the two post-reaction Marcellus-PA samples. The post-reaction Marcellus-PA with a layer of barite scale formed at the shale-fluid interface had less pyrite oxidation in the matrix, likely because the barite layer reduced transport rate of dissolved oxygen into the matrix. Condition 1 refers to reactions in fracture fluid, and Condition 2 refers to reactions in fracture fluid with additional Ba^{2+} and SO_4^{2-} to form barite. The color scale for Marcellus-PA is different from the other two shales.

For Eagle Ford shale, Figure 3 shows that there is no noticeable difference between reacted and un-reacted shale (Condition 1) except that the sulfate in barite precipitation is captured when Ba^{2+} and SO_4^{2-} were added to form barite (Condition 2). The location where sulfate in barite is observed is consistent with the µ-CT cross-sectional slice shown in Figure 2. The limited pyrite oxidation in the Eagle Ford matrix is explained by the pH dependence of Fe(II) oxidation. Oxidation of Fe(II) by dissolved O_2 is much faster at high pH than low pH. When pH of the Eagle Ford was neutralized due to fast carbonate dissolution, Fe(II) released from pyrite oxidation can be quickly oxidized, consuming dissolved oxygen and leaving limited oxygen to diffuse further into the matrix to oxidize pyrite there. But in the Marcellus system where pH remained low, Fe(II) oxidation is much slower, oxygen was mostly consumed by pyrite dissolution according to Eq. 1, leaving much of the Fe species in the ferrous form. If there is continuous supply of dissolved oxygen, such as at the locations near the injection point, ferrous Fe can further be oxidized to form ferric scales, with the potential to reduce gas and oil transport through matrices and fractures.

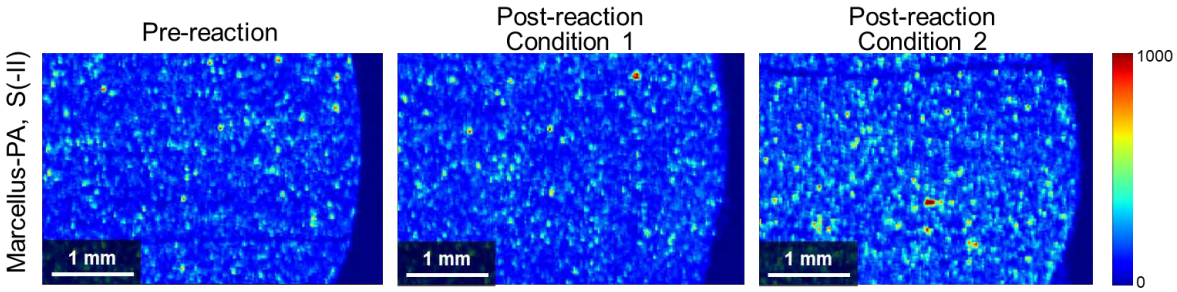

Figure 4. Synchrotron µ-XRF sulfide maps taken at 2471.5 eV. The difference among pre-reaction and post-reaction samples is attributed to shale heterogeneity. Although pyrite oxidation occurred throughout the Pennsylvania Marcellus cores, the amount of pyrite did not decrease apparently, suggesting only a small fraction of pyrite was oxidized.

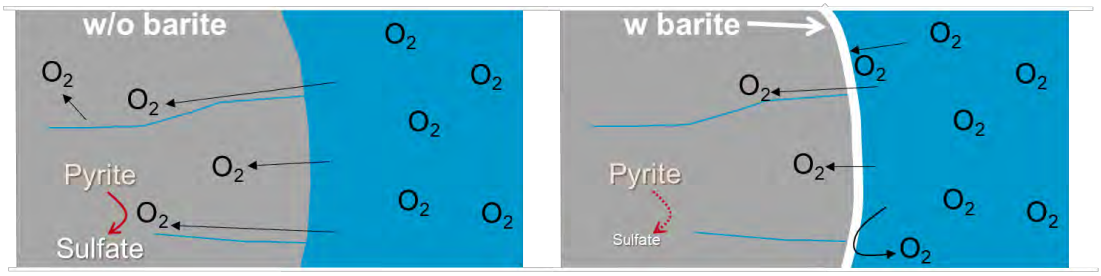

Figure 5. Illustration of the effect of barite scale in reducing transport of dissolved oxygen, and possibly also gas/oil, across the shale-fluid interface.

Conclusions

Our study demonstrated that shale matrices can be more reactive than commonly thought. The reaction penetration depths into the matrix depend on the amount of microcracks, mineralogical composition, reaction types, and on fracture fluid composition, namely pH, scale forming ions, and dissolved oxygen.

When comparing pyrite oxidation in New York Marcellus cores and Pennsylvania Marcellus cores, it is evidenced that microcracks acted as important channels for reactive chemicals to migrate deep into the shale matrix. In addition to microcracks, other types of connected porosity serve as complementary pathways for chemicals to transport to a wider zone in the shale interior. Because of the availability of connected porosity such as microcracks in the Pennsylvania Marcellus sample, pyrite oxidation occurred at least 5 mm into the matrix after 3 weeks of reaction with fracture fluid.

For barite precipitation, the reaction depth was 2–3 mm into the matrix for carbonate-rich Eagle Ford after three weeks, but was only about 30–40 µm at the shale-fluid interfaces for carbonate-poor Marcellus samples. The strikingly more abundant barite precipitation in the Eagle Ford system compared to either of the Marcellus systems

was due to the higher pH by carbonate dissolution in the Eagle Ford system, which favored faster and more barite formation. Both microcracks and the relatively high local pH in the microcracks and matrix pores were important for barite precipitation to occur in the matrix.

The chemical reactions in shale matrices can alter pore structure and wettability and alter transport behavior of hydrocarbon. Understanding the types and depths of chemical reactions can help refine reactive transport models to predict their impact on gas/oil production, leading to optimization of fracture fluid chemistry for unconventional resource stimulation.

Acknowledgments

This work was funded by NETL to SLAC under Contract #DE-AC02-765F00515. SSRL is a national user facility supported by the DOE Office of Basic Energy Sciences. We also acknowledge Stanford Nano Shared Facilities (SNSF) for providing shared access to the ZEISS Xradia 520 Versa 3D X-ray microscope. SNSF is supported by the NSF under award ECCS-1542152.

References

Al Ismail, M. I. and M. D. Zoback (2016). "Effects of Rock Mineralogy and Pore Structure on Stress-Dependent Permeability of Shale Samples." *Philosophical Transactions of the Royal Society A* **374**(2078): 20150428.

Alalli, A., Q. Li, A. Jew, A. Kohli, J. R. Bargar and M. Zoback (2018). Effects of Hydraulic Fracturing Fluid on Shale Matrix Permeability. *Unconventional Resources Technology Conference (URTEC)*, Houston, Texas, USA.

Carter, K. M., J. A. Harper, K. W. Schmid and J. Kostelnik (2011). "Unconventional Natural Gas Resources in Pennsylvania: The Backstory of the Modern Marcellus Shale Play." *Environmental Geosciences* **18**(4): 217-257.

Dehghanpour, H., Q. Lan, Y. Saeed, H. Fei and Z. Qi (2013). "Spontaneous Imbibition of Brine and Oil in Gas Shales: Effect of Water Adsorption and Resulting Microfractures." *Energy & Fuels* **27**(6): 3039-3049.

Dehghanpour, H., H. Zubair, A. Chhabra and A. Ullah (2012). "Liquid Intake of Organic Shales." *Energy & Fuels* **26**(9): 5750-5758.

Dieterich, M., B. Kutchko and A. Goodman (2016). "Characterization of Marcellus Shale and Huntersville Chert Before and After Exposure to Hydraulic Fracturing Fluid via Feature Relocation Using Field-Emission Scanning Electron Microscopy." *Fuel* **182**: 227-235.

Dove, P. M. and C. A. Czank (1995). "Crystal Chemical Controls on the Dissolution Kinetics of the Isostructural Sulfates: Celestite, Anglesite, and Barite." *Geochimica et Cosmochimica Acta* **59**(10): 1907-1915.

Fathi, E. and I. Y. Akkutlu (2009). "Matrix Heterogeneity Effects on Gas Transport and Adsorption in Coalbed and Shale Gas Reservoirs." *Transport in Porous Media* **80**(2): 281.

Grieser, W. V., W. E. Wheaton, W. D. Magness, M. E. Blauch and R. Loghry (2007). Surface Reactive Fluid's Effect on Shale. *Production and Operations Symposium*, Society of Petroleum Engineers.

Gu, X., D. R. Cole, G. Rother, D. F. Mildner and S. L. Brantley (2015). "Pores in Marcellus Shale: A Neutron Scattering and FIB-SEM Study." *Energy & Fuels* **29**(3): 1295-1308.

Guo, C., M. Wei and H. Liu (2015). "Modeling of Gas Production From Shale Reservoirs Considering Multiple Transport Mechanisms." *PLOS One* **10**(12): e0143649.

Hammack, R., W. Harbert, S. Sharma, B. Stewart, R. Capo and A. Wall (2014). An Evaluation of Fracture Growth and Gas/Fluid Migration as Horizontal Marcellus Shale Gas Wells are Hydraulically Fractured in Greene County, Pennsylvania. National Energy Technology Laboratory: NETL-TRS-3-2014, 76pp. .

Harrison, A. L., A. D. Jew, M. K. Dustin, D. L. Thomas, C. M. Joe-Wong, J. R. Bargar, N. Johnson, G. E. Brown and K. Maher (2017). "Element Release and Reaction-Induced Porosity Alteration During Shale-Hydraulic Fracturing Fluid Interactions." *Applied Geochemistry* **82**: 47-62.

He, C., M. Li, W. Liu, E. Barbot and R. D. Vidic (2014). "Kinetics and Equilibrium of Barium and Strontium Sulfate Formation in Marcellus Shale Flowback Water." *Journal of Environmental Engineering* **140**(5): B4014001.

Heller, R., J. Vermylen and M. Zoback (2014). "Experimental Investigation of Matrix Permeability of Gas Shales." *AAPG Bulletin* **98**(5): 975-995.

Huang, X., K. W. Bandilla and M. A. Celia (2016). "Multi-Physics Pore-Network Modeling of Two-Phase Shale Matrix Flows." *Transport in Porous Media* **111**(1): 123-141.

Jew, A. D., M. K. Dustin, A. L. Harrison, C. M. Joe-Wong, D. L. Thomas, K. Maher, G. E. Brown Jr and J. R. Bargar (2017). "Impact of Organics and Carbonates on the Oxidation and Precipitation of Iron During Hydraulic Fracturing of Shale." *Energy & Fuels* **31**(4): 3643-3658.

Kan, A. and M. Tomson (2012). "Scale Prediction for Oil and Gas Production." *SPE Journal* **17**(02): 362-378.

Karra, S., N. Makedonska, H. S. Viswanathan, S. L. Painter and J. D. Hyman (2015). "Effect of Advective Flow in Fractures and Matrix Diffusion on Natural Gas Production." *Water Resources Research* **51**(10): 8646-8657.

Kuuskraa, V., S. H. Stevens and K. D. Moodhe (2013). Technically Recoverable Shale Oil and Shale Gas Resources: An Assessment of 137 Shale Formations in 41 Countries Outside the United States, US Energy Information Administration, US Department of Energy.

Marcon, V., C. Joseph, K. E. Carter, S. W. Hedges, C. L. Lopano, G. D. Guthrie and J. A. Hakala (2017). "Experimental Insights into Geochemical Changes in Hydraulically Fractured Marcellus Shale." *Applied Geochemistry* **76**: 36-50.

Moghadasi, J., M. Jamialahmadi, H. Müller-Steinhagen, A. Sharif, A. Ghalambor, M. Izadpanah and E. Motaie (2003). Scale Formation in Iranian Oil Reservoir and Production Equipment During Water Injection. *International Symposium on Oilfield Scale*, Society of Petroleum Engineers.

Palandri, J. L. and Y. K. Kharaka (2004). A Compilation of Rate Parameters of Water-Mineral Interaction Kinetics for Application to Geochemical Modeling, Geological Survey Menlo Park CA.

Pournik, M. and D. Tripathi (2014). Effect of Acid on Productivity of Fractured Shale Reservoirs, Unconventional Resources Technology Conference (URTEC).

Steefel, C. (2009). "CrunchFlow. Software for Modeling Multicomponent Reactive Flow and Transport. User's Manual." *Earth Sciences Division. Lawrence Berkeley, National Laboratory, Berkeley, CA. October*: 12-91.

Swami, V. and A. Settari (2012). A Pore Scale Gas Flow Model for Shale Gas Reservoir. *SPE Americas Unconventional Resources Conference*, Society of Petroleum Engineers.

Vankeuren, A. N. P., J. A. Hakala, K. Jarvis and J. E. Moore (2017). "Mineral Reactions in Shale Gas Reservoirs: Barite Scale Formation From Reusing Produced Water as Hydraulic Fracturing Fluid." *Environmental Science & Technology* **51**(16): 9391-9402.

Villazon, M., G. German, R. F. Sigal, F. Civan and D. Devegowda (2011). Parametric Investigation of Shale Gas Production Considering Nano-Scale Pore Size Distribution, Formation Factor, and Non-Darcy Flow Mechanisms. *SPE annual technical conference and exhibition*, Society of Petroleum Engineers.

Wu, W. and M. M. Sharma (2017). "Acid Fracturing in Shales: Effect of Dilute Acid on Properties and Pore Structure of Shale." *SPE Production & Operations* **32**(01): 51-63.

Zhang, P., L. Hu, J. N. Meegoda and S. Gao (2015). "Micro/Nano-Pore Network Analysis of Gas Flow in Shale Matrix." *Scientific Reports* **5**: 13501.